INSTITUTE OF PHYSICS PUBLISHING JOURNAL OF PHYSICS D: APPLIED PHYSICS

J. Phys. D: Appl. Phys. **34** (2001) 560–566 www.iop.org/Journals/jd PII: S0022-3727(01)16772-0

Space- and time-resolved soft x-ray emission from laser-produced magnesium plasma

S S Harilal, C V Bindhu and H-J Kunze

Institut für Experimentalphysik V, Ruhr-Universität Bochum, Universitätsstrasse 150, D-44780 Bochum, Germany

E-mail: hans-joachim.kunze@ep5.ruhr-uni-bochum.de

Received 31 August 2000, in final form 27 November 2000

Abstract

Soft x-ray emission from plasmas produced by ablation from a magnesium target employing a ruby laser is studied using a grazing incidence spectrograph in the spectral region 3–12 nm. Emission intensities are investigated for different ionic lines as a function of position, time after the maximum of the laser pulse and laser irradiance. A gated pinhole camera is employed for studying the evolution of the plasma at early stages. The propagation distances and velocities are measured. Our results show that the line intensities of all ionic lines increase with laser irradiance until a saturation plateau is observed at high irradiance levels. The increase in ionization and intensity saturation with varying laser irradiance seems to suggest strong interaction of the laser pulse with the dense plasma formed near the target within the pulse duration.

(Some figures in this article are in colour only in the electronic version; see `www.iop.org`)

1. Introduction

High-power short laser pulses have been extensively applied to ablate solid materials for thin-film deposition, material processing, production of clusters and nanotubes, etc. Because of the technological importance of the ablation process, many efforts have been made towards the understanding of the hydrodynamics of laser-induced plasmas [1–3]. There are several dynamic processes involved in a laser ablation mechanism which include explosive removal of material, laser plasma interaction and strong collisions among plasma species. The nature and dynamics of the laser-produced plasmas vary with different experimental parameters, which include laser parameters such as: wavelength; irradiance; pulse shape; spot size on the target; target material characteristics such as composition and their thermal as well as optical properties; pressure and nature of the background gas, etc. Various theories have been proposed for understanding plume dynamics and assessing plasma properties such as temperature, pressure and density distributions [4–7]. The study of basic mechanisms involved in the laser ablation process is an important task, since the underlying processes still are not fully understood [8–14].

Laser matter interaction is a complex phenomenon involving various aspects of heat transfer, melting, vaporization, gas dynamics and plasma formation. Most of the reported studies mainly concern the later stages of the plasma expansion, i.e. times >100 ns after the initial impact of the laser onto the target surface and the initialization of the plasma. But laser ablation is a complicated process in the early stages of ablation <100 ns. Only limited reports have been found for laser-produced plasma diagnostics at delay times less than 100 ns [15, 16]. Most of the established diagnostic techniques, such as optical emission spectroscopy, mass spectroscopy, Langmuir probe etc, are not suitable for studying the dynamics of the plasma, especially at the early stages. Also, optical emission diagnostic techniques are not suitable since at early stages the measurements can be affected by the intense continuum background, as well as the possibility of self-absorption [14, 17]. In the cases of mass spectroscopy and Langmuir probe, the detector/probe is placed at a certain distance away from the target surface and the detected signal is delayed by a few microseconds after the laser irradiation. Hence, they cannot reflect the early stages of ablation [9, 18].

The study of soft x-ray and XUV emission spectra from laser-produced plasmas is of considerable importance in the fields of laser-driven inertial confinement fusion, x-ray lasers and soft x-ray lithography [19–21]. For laser-produced

plasmas, several types of extreme UV and soft x-ray spectrographs have been constructed. Although several different types of XUV spectrograph based on grazing incidence geometry can be used to achieve high spectral resolution [22–24], transmission grating spectrographs operating at normal incidence have been used extensively to cover a wide spectral region with moderate resolution [25,26]. Boland *et al* [27] studied laser-produced plasma from polyethylene with a space-resolved spectroscopic technique using a 2 m grazing incidence spectrograph. Their results had no experimental time resolution but they followed a particular ion species during expansion. Irons *et al* [28] used a grazing incidence spectrograph for studying the plasma produced by laser irradiation of polyethylene foil in vacuum in a time integrated manner. More recently, many studies on coherent XUV generation have been reported with ultra-short lasers using XUV grazing incidence spectrographs [29].

In this paper, we have investigated temporally and spatially resolved emission by means of a grazing incidence spectrograph equipped with a microchannel plate having gating functions. The aim of this work was to use soft x-ray spectroscopy methods to diagnose early phases of the laser plasma (<50 ns). A pinhole camera is used to image the plasma for investigating the early dynamics of the laser plasma plume. An aluminium filter limited the observed radiation to the soft x-ray and XUV regions; hence the images represent only the hot plasma region. As XUV radiation is emitted only by hot and dense plasmas where higher ionization stages dominate, this technique is suitable for studying the plasma plume in the early stages.

2. Experimental set-up

A schematic diagram of the experimental set-up has been given in a recent paper [30]. The radiation from a ruby laser (693.4 nm, maximum energy 6 J, pulse width 15 ns) is focused at right angles to the target surface (magnesium, purity 99.9%, thickness 1 mm) with the use of a plano-convex lens of 300 mm focal length. The estimated focal spot at the target surface is ∼400 μm in diameter. The target is placed in a high vacuum chamber evacuated to a background pressure of 10^{-5} Torr. The target slab is placed on an X–Y motorized linear mount so that a fresh surface is presented to the laser for each shot. This prevents the creation of craters that will occlude emission from the hot core of the plasma. For spectral studies, a gold-coated spherical mirror with 4 m radius of curvature is used to image the emitted radiation on the entrance slit of the grazing incidence spectrograph. The mirror was placed equidistant between the plasma and the entrance slit of the spectrograph. This set-up essentially provides spatial resolution to better than 200 μm. No contamination of the mirror by plasma debris was observed. The spectrograph is equipped with a concave grating with a 5649 mm radius of curvature and set for an angle of incidence on the grating of 87°. The gold-plated grating with varying groove spacing (1095–1450 l mm^{-1}) focuses the spectrum on a flat plane instead of on the Rowland circle. The spectrograph covers the spectral range from 3–25 nm at moderate wavelength resolution (typically $\lambda/\Delta\lambda = 1100$ at a slit width of 10 μm). To detect soft x-rays in the 3–12 nm wavelength range, we used a flat microchannel plate (MCP) detector combined with a cooled charged-coupled device (CCD) assembly. The CCD detector is connected to a computer equipped with software for data acquisition and spectral analysis. The wavelength calibration of the monochromator was carried out by plasma spectroscopy using a carbon target.

High-speed photography of the plume is performed using a gated pinhole camera. For this we used a 50 μm pinhole with a microchannel plate combined with a CCD. The pinhole camera had an aluminium filter (27 mg cm^{-3}), resulting in a spectral sensitivity of the system to the region <80 nm. The camera provides two-dimensional intensity distribution measurements of the plume integrated over the XUV and EUV spectral range.

3. Results and discussion

3.1. XUV photography

As the laser intensity exceeds the ablation threshold of the target, the laser beam evaporates and ionizes the material, creating a plasma plume above the material surface. The resulting plasma expands away from the target in a direction perpendicular to the target surface. Pinhole images are taken during the early stages, which provides an orthogonal view of the expansion with respect to the target plane. The pinhole camera is placed at a distance 5 cm away from the laser spot. The image of the expanding plume is recorded by an MCP-CCD system described above, which is placed at a distance of 45 cm from the pinhole, resulting in a magnification of nine on the detection plane. Typical CCD images of the expanding XUV plume at different times after the maximum of the laser pulse are given in figure 1 recorded at a laser irradiance of 2.2×10^{11} W cm^{-2}. The gating time is 5 ns (given by experimental restraints) and each image is obtained from a single laser pulse. The greyscale palette of the pictures is representative of the light intensity measured by the camera. Initially, the atoms, molecules and ions undergo collisions in the high-density region near the target, forming the so-called Knudsen layer, to create a highly directional expansion perpendicular to the target [31]. After that, the particles slow down and move with almost constant velocity as a result of velocity equalizing collisions between fast and slow particles.

The expansion dynamics of the laser-produced plasma plume has been described elsewhere using semiquantative models [32, 33]. The theoretical treatments describe the particle motion in the perpendicular direction (Z) and two lateral directions (X and Y) with respect to the target plane. In the initial stage, the interaction of the laser beam with the bulk target results in the evaporation of the surface layer. Following this, the interaction of the laser beam with the evaporating material leads to the formation of an isothermally expanding plasma and this persists until the termination of the laser pulse. The dimension of the plume during isothermal expansion ($t \leqslant \tau$, τ being the pulse width of the laser), is given by [33],

$$X(t)\left[\frac{1}{2t}\frac{\mathrm{d}X}{\mathrm{d}t}+\frac{\mathrm{d}^2X}{\mathrm{d}t^2}\right]=Y(t)\left[\frac{1}{2t}\frac{\mathrm{d}Y}{\mathrm{d}t}+\frac{\mathrm{d}^2Y}{\mathrm{d}t^2}\right]$$
$$=Z(t)\left[\frac{1}{2t}\frac{\mathrm{d}Z}{\mathrm{d}t}+\frac{\mathrm{d}^2Z}{\mathrm{d}t^2}\right]=\frac{kT_0}{M} \qquad (1)$$

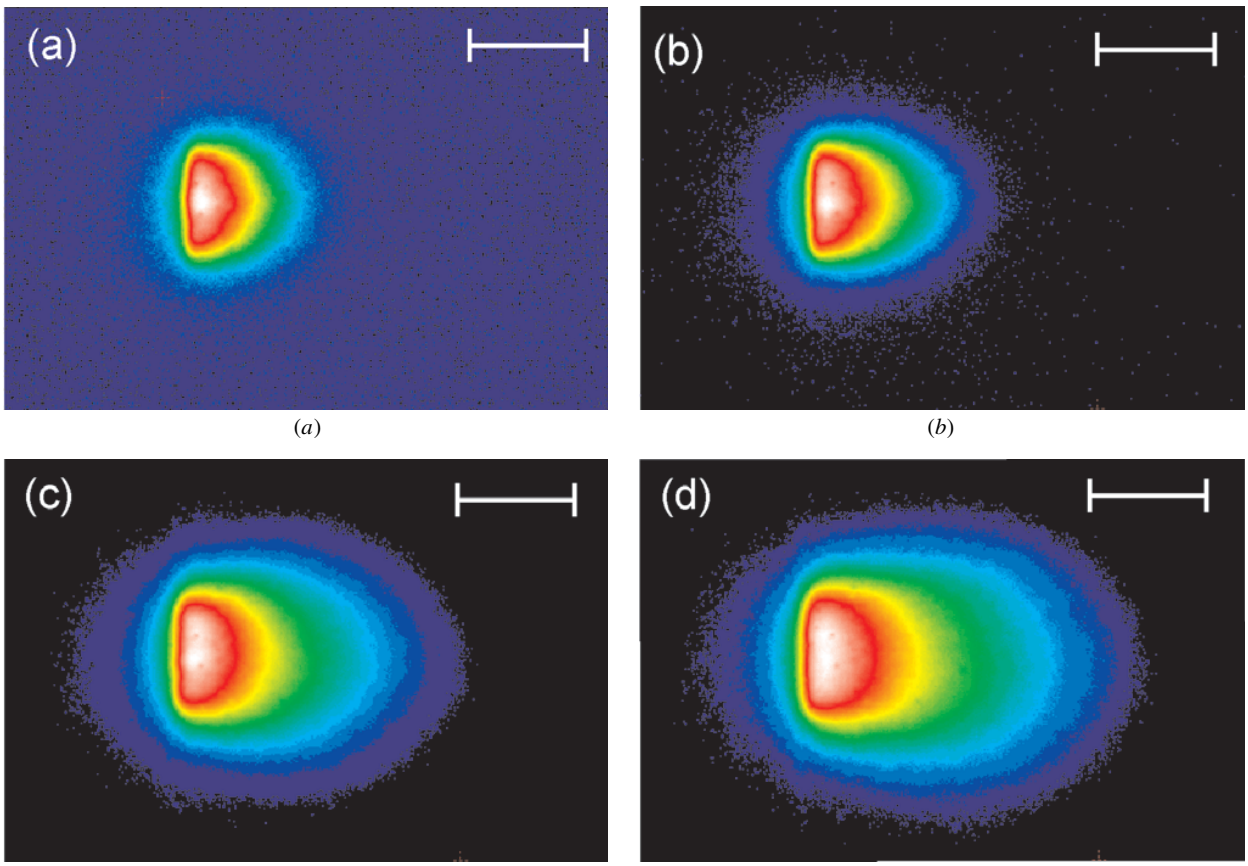

(*a*) (*b*) (*c*) (*d*)

Figure 1. Typical XUV pinhole images of the expanding magnesium plasma at various delays: (*a*) 4 ns; (*b*) 7 ns; (*c*) 16 ns; (*d*) 21 ns. The time represents the evolution of the plasma after the maximum of the laser pulse. The scale in the images corresponds to 500 μm.

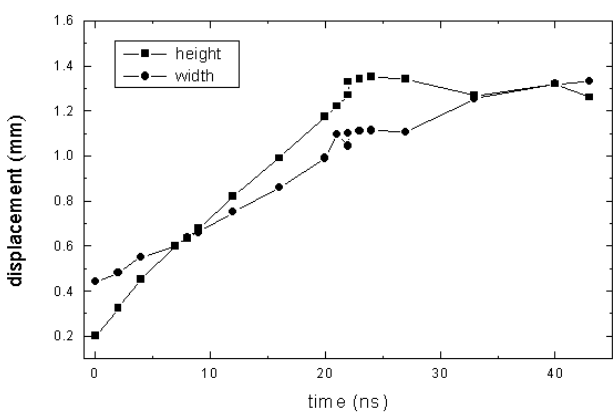

Figure 2. Displacement–time plot for XUV images of laser produced magnesium plasma in the Z (height) and Y (width) directions. The plume height and width are taken along with outermost axial position where the intensity falls to 10% of the maximum intensity.

where $X(t)$, $Y(t)$ and $Z(t)$ represent the three mutually perpendicular expansion directions, $\mathrm{d}X/\mathrm{d}t$, $\mathrm{d}Y/\mathrm{d}t$ and $\mathrm{d}Z/\mathrm{d}t$ are the respective expansion velocities of the plasma edges X, Y and Z respectively, k is the Boltzmann constant, T_0 is the isothermal temperature and M is the mass of the particle. As the velocities are controlled by the pressure gradients, the expansion is anisotropic in the direction perpendicular to the target surface. When the pulse terminates, the regime changes to unsteady adiabatic expansion (UAE). A similar equation, where no injection of particles is taken into account, controls the expansion of the plasma in this regime ($t \geqslant \tau$), and is given by [33],

$$X(t)\left[\frac{\mathrm{d}^2X}{\mathrm{d}t^2}\right] = Y(t)\left[\frac{\mathrm{d}^2Y}{\mathrm{d}t^2}\right] = Z(t)\left[\frac{\mathrm{d}^2Z}{\mathrm{d}t^2}\right] = \frac{kT_0}{M}\left[\frac{X_0Y_0Z_0}{X(t)Y(t)Z(t)}\right] \tag{2}$$

where X_0, Y_0 and Z_0 are the orthogonal edges of the plume when $t = \tau$. Figure 2 represents the XUV plume height (Z) and width (Y) with respect to time measured from the pinhole images. Initially, the height of the plume is less than the width of the spot size in the present investigation, which is ~400 μm. It is worth noting that the XUV plume length increases with time until 20 ns after the maximum of the laser pulse, after that it rolls off. As the height of the plume increases with time from the beginning of the observation, we can conclude that the material is ejected in a direction normal to the target surface, then the plume expands in the three directions of the space. So the laser-produced plasma shows an elliptical shape which contours along the propagation direction. The phenomenom is mainly due to the initial gradients of the density and pressure in the plasma plume which are much larger in a direction perpendicular to the target surface than those in the lateral direction [34].

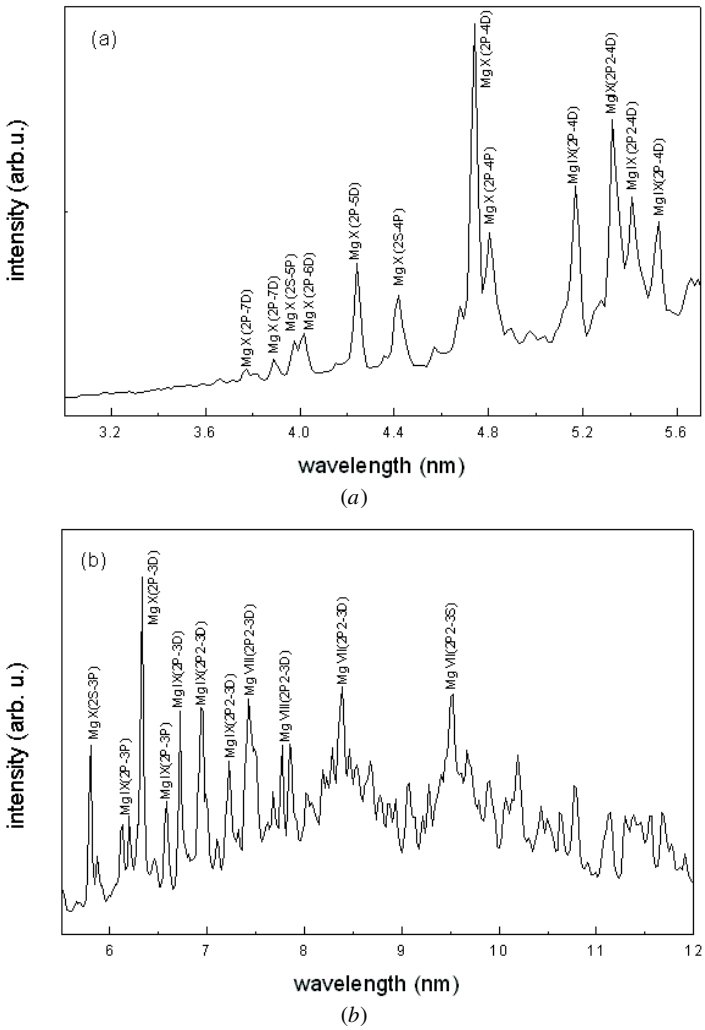

Figure 3. Soft x-ray spectrum of a magnesium plasma obtained at a distance 5 mm from the target surface, 5 ns after the maximum of the laser pulse and at a laser irradiance of 2.5×10^{11} W cm^{-2}: (*a*) spectrum covers the region 3–5.5 nm and (*b*) the region 5.5–12 nm.

The pinhole images give the temporal variation of the displacement of the plume front and hence the velocity of the plume. The expansion velocities of the plasmas are measured from the time evolution of the pinhole pictures (slopes of the displacement–time graph given in figure 2). The estimated expansion velocities of the plasma in the initial stages are 4.6×10^6 cm s^{-1} and 2.9×10^6 cm s^{-1} in the Z and Y directions, respectively. As the expansion velocity of the plasma in the Z direction is higher than that of the corresponding value in the lateral direction, we can conclude that the preferential expansion is in the direction normal to the target surface. The XUV plume length in a ns laser-ablated plasma is limited to within 2 mm from the target surface and to a less than 100 ns lifetime compared to a 5–6 cm plume length and to a tens of microseconds lifetime observed in the visible spectroscopic region [34].

3.2. Soft x-ray spectral studies

Line emission from highly charged ions in the soft x-ray region represents an important diagnostics of high-temperature plasmas. Laser-produced plasmas are considered to be one of the best sources of x-rays, soft x-rays and XUV radiation [35]. Spectral measurements have been performed to investigate the dynamics of the highly charged ions in laser-produced magnesium plasma in the wavelength region 3–12 nm. Typical emission spectra of the plasma produced by laser ablation of magnesium in vacuum recorded at a distance of 0.75 mm from the target surface are given in figure 3. Lines are identified from the literature [36, 37] and their assignments are given in the figure. Owing to the very large number of lines present, the spectra are very crowded especially at the red end of the observed region. Usually, plasma parameters, namely electron temperature and density, are estimated by assuming the plasma to be in local thermodynamic equilibrium (LTE). In a transient high density system, such as the plasma formed by a pulsed laser beam, LTE is said to exist if the collisional de-excitation is much more rapid than radiative de-excitation [38]. Assuming LTE as a coarse approximation, we estimated an electron temperature of the plasma $\sim 40 \pm 10$ eV at a distance 0.5 cm from the target surface. The determination of the plasma parameters during the early stages is difficult because of the high optical thickness of the spectral lines emitted from the initial dense plasma [30]. The ejected plasmas have a highly directed kinetic energy as well as density gradients, which will reduce the effective optical depth appreciably.

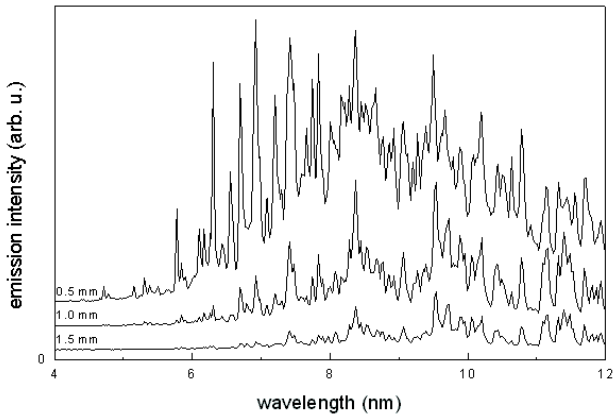

Figure 4. Plasma spectra recorded at different distances from the target surface. The spectra are recorded 8 ns after the maximum of the laser pulse and at a laser irradiance 2.2×10^{11} W cm^{-2}.

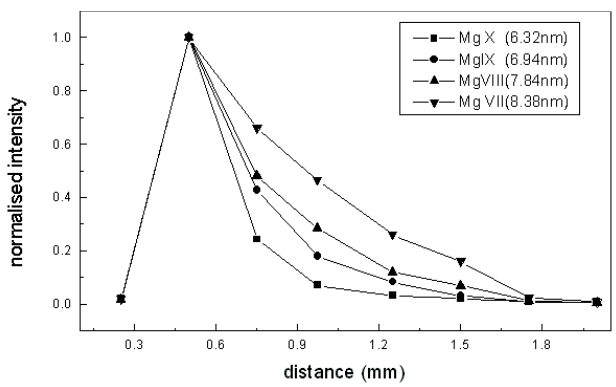

Figure 5. Change in emission intensity with distance for different ionic species.

The temperature measurements can also be affected, with a large error due to a small separation of the upper levels. Nevertheless, these measurements were rough estimations and do not take into account self-absorption of the lines.

Space-resolved spectral measurements are made by setting the gate width to 10 ns. Figure 4 gives the spectral emission from laser-induced magnesium plasmas recorded at different distances from the target surface. The spectra are recorded 8 ns after the maximum of the laser pulse and at a laser irradiance of 2.2×10^{11} W cm^{-2}. The continuum emission intensity in the plasma centred around 8 nm is greatest in the region close to the target surface. The continuum arises as a result of free–free bremsstrahlung and electron–ion recombination. Spectral analysis shows the presence of intense line emission from Li-like and Be-like Mg ions close to the target surface along with Mg VIII and Mg VII. At larger distances, the spectra are dominated by lowly charged ions (Mg VIII–V). Figure 5 gives the change in intensity with distance for different ionic species of magnesium. The maximum spatial range for the ions is limited by the drop in recorded intensity with distance.

To understand the detailed aspects of laser-beam interaction with the target material and recombination processes following the laser ablation, time-resolved studies of the emission spectra from the plasma offer the most convenient approach [39]. Time-resolved spectra are recorded

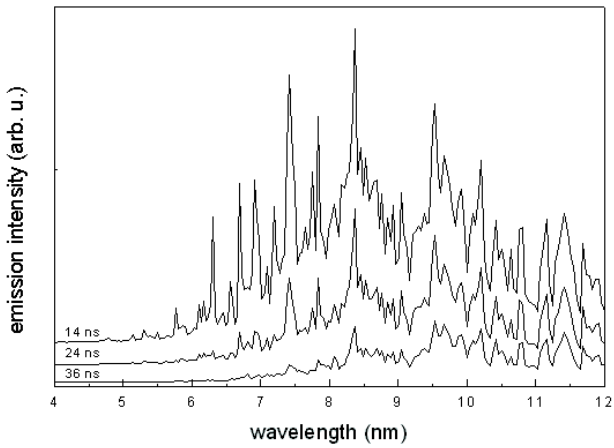

Figure 6. Plasma emission spectra in the wavelength range 4–12 nm at different time delays. The time delays correspond to the time after the maximum of the laser pulse. The spectra are charted at a distance of 0.75 mm away from the target surface and at a laser irradiance of 2.2×10^{11} W cm^{-2}.

by setting the gate width to 10 ns and choosing a section 0.75 mm away from the target surface at a laser irradiance of 2.2×10^{11} W cm^{-2}. Typical spectra, as recorded under different regimes of the plasma expansion, are shown in figure 6. Figure 7 gives the temporal variation of normalized emission intensity for different ionic states. Ionic lines are characterized by a narrower temporal distribution with an increasing degree of ionization. From figure 7, it is clear that the emissions of all ionic stages are delayed by 14 ns after the maximum of the laser pulse, which is contrary to normal observation. In actual practice, the species with a higher degree of ionization have higher velocities because of the Coulomb fields generated by negatively charged electrons escaping from the plume. The observed phenomenon is expected to be due to a lack of time resolution used in the present studies. Assuming that the maximum emission intensity at a given distance corresponds to the time when the plasma front passes through the observation zone, the velocity of the plasma front in the direction perpendicular to the target surface can be estimated from figure 7 to a value of about 5×10^6 cm s^{-1}. This expansion velocity calculated from the time-resolved spectral studies matches well with expansion velocities estimated from the pinhole pictures.

We also investigated the effect of laser irradiance on the emission from the different ionic lines. The spectra are recorded at a distance of 0.75 mm from the target surface and gated 8 ns after the maximum of the laser pulse (gate width 10 ns). Figure 8 gives the normalized magnesium ion intensities with laser irradiance. Initially, with increasing laser irradiance, a monotonic increase in emission intensity is observed for all ions up to a laser irradiance 2×10^{11} W cm^{-2}. After that, the intensities from different ions show a sudden enhancement in intensity. As laser irradiance increases, the number of free electrons also increases and consequently the electron density as well. The electrons also gain energy from the oscillation field due to random collisions with plasma species. An increase in the electron energy leads to further ionization and formation of dense plasma by photo-ionization, multi-photon ionization and ionization by electron impact.

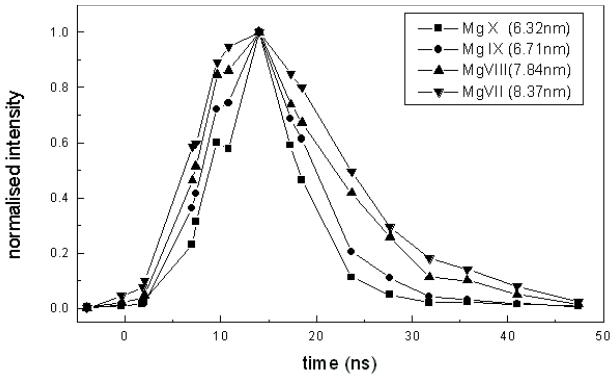

Figure 7. Normalized emission intensity for different ionic species with time.

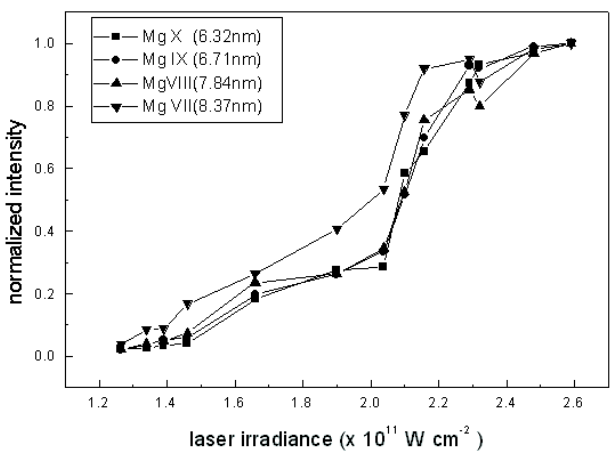

Figure 8. Change in intensity with laser irradiance for different ionic species.

The process of optical breakdown and plasma formation is due to avalanche ionization for long wavelength (IR and VIS) and multi-photon ionization for short wavelength lasers (UV). The 'quiver' energy of a free electron oscillating in an electromagnetic field is given by [40, 41]

$$U_{\rm os} = \frac{e^2E^2}{2m\omega^2} \tag{3}$$

where ω is the angular frequency of the laser field. By substituting the experimental parameters the calculated $U_{\rm os}$ is only $\sim 10^{-2}$ eV, i.e. too low. Although hot electrons with much higher kinetic energies can be generated by the resonance absorption of laser radiation, we exclude this possibility here because resonance absorption phenomena will take place only when the laser beam is incident obliquely on the target [42, 43]. Moreover, resonance absorption phenomena in laser-produced plasmas usually take place at high laser intensities ($\sim 10^{14}$ W cm^{-2} or higher) [44, 45] in comparison with the laser irradiance $\sim 10^{11}$ W cm^{-2} used in the present studies.

At higher laser irradiance levels, a saturation phenomenon is observed for all emission lines irrespective of their ionization levels. The increase in ionization and intensity saturation with varying laser irradiance seems to suggest strong interaction of the laser pulse with dense plasma formed at the target surface within the pulse duration. The saturation in the emission lines at higher laser irradiance levels is expected to be due to plasma shielding, i.e. absorption and/or reflection of the laser photons by the plasma itself. In the present investigation, the pulse duration of the laser used is relatively long (15 ns), and this allows an efficient coupling with the plasma before the pulse terminates. The reflection of the incident photons takes place when the plasma frequency $\nu_{\rm p} \geqslant$ laser frequency $\nu_{\rm l}$. In the present case, the calculated plasma frequency (assuming an electron density of $\sim 5 \times 10^{19}$ cm^{-3}) is one order smaller than the laser frequency. So, the energy losses due to the reflection of the laser beam from the plasma can be assumed to be insignificant. The dominant mechanism responsible for plasma absorption at these laser irradiance levels is inverse bremsstrahlung. Since the excitation and ionization potential of magnesium is much greater than the pump photon energy (1.8 eV) direct photo-ionization by the absorption of a laser photon is ruled out. Besides, photo-ionization, impact ionization and thermal ionization, etc, may also affect the absorption coefficient of the plasma. The inverse bremsstrahlung process due to electron–ion scattering is usually described by the inverse absorption length, which is given by [46]

$$\sigma_{\rm ib} \approx 1.27 \times 10^{-46}\lambda^3 Z^2 n_{\rm e} n_{\rm i} T_{\rm e}^{-1/2}\left[1 - \exp\left(-\frac{h\nu}{T_{\rm e}}\right)\right] \tag{4}$$

where λ is the wavelength of the laser photons in nm, $T_{\rm e}$ is the electron temperature in eV, $h\nu$ is the laser photon energy in eV, Z is the ionic charge and $n_{\rm i}$ and $n_{\rm e}$ are the ion and electron densities, respectively. From equation (4) it is clear that inverse bremsstrahlung is an efficient absorption process especially at visible and IR wavelengths, because of its wavelength dependence of λ^3. With increasing laser irradiance, more excited species, ions and free electrons are generated that interact with incoming laser photons, leading to further heating and ionization and resulting in an increase in absorption of the laser energy. The plasma progressively behaves like an optically thick medium and effectively shields the target surface from the trailing part of the laser pulse. During this process, a self-regulating regime may exist when an appreciable amount of laser energy is absorbed by the plasma. Amoruso *et al* [47] also observed a saturation in the collected ion yield at high irradiance levels with second and third harmonics of Nd:YAG laser-ablated aluminium plasma. They ascribed it due to strong absorption and partial or total reflection of the laser light by the hot plasma produced by the leading edge of the pulse.

4. Summary

We have used XUV photographic techniques to study the temporal evolution of expanding laser-ablated magnesium plasmas. XUV pinhole pictures of plasmas reveal more details about the expansion dynamics of the plasma plume at the early stages. The results are compared to time-resolved spectroscopic measurements in the soft x-ray region. It is observed that the highest velocities are in the direction of the smallest dimensions of the laser spot which gives an elliptical plume expanding away from, and normal to, the target surface. Spectral analysis shows the presence of intense line emission

from Li-like and Be-like Mg ions close to the target surface along with Mg VIII and Mg VII. Spatial studies reveal that the yield of soft x-ray photons is limited to within 2 mm from the target surface and to <50 ns after the maximum of the laser pulse. Time-resolved studies show that these ions have high expansion velocities which give rise to a kinetic energy ∼300 eV. The results of time-resolved spectra are consistent with those obtained from pinhole experiments using an aluminium filter. We observed saturation in the emission intensity for different ionic stages at high laser irradiance levels. At low laser irradiance, the laser photons completely reach the target surface, but at high irradiance levels, because of absorption of the laser photons by the plasma, the effective laser–target coupling is reduced. With an increase in laser irradiance, more excited species, ions and free electrons are generated that interact with incoming laser photons, leading to further heating and ionization and resulting in an increase of the absorption of the laser photons.

Acknowledgment

One of us (SSH) thanks the Alexander von Humboldt Foundation, Germany for a research fellowship.

References

[1] Geohegan D B 1994 *Pulsed Laser Deposition of Thin Films* ed D B Chrisey and G K Hubler (New York: Wiley)
[2] Takabe H, Nagatomo H, Sunahara A, Ohnishi N, Mahdy A I, Yoda Y, Naruo S, Azechi H, Nishimura H and Mima K 1999 *Plasma Phys. Control. Fusion* **41** A 75
[3] Amoruso S, Bruzzese R, Spinelli N and Velotta R 1999 *J. Phys. B: At. Mol. Opt. Phys.* **32** R131
[4] Guidoni A G, Kelly R, Mele A and Miotello A 1997 *Plasma Sources Sci. Technol.* **6** 260
[5] Neamtu J, Mihailescu I N, Ristoscu C and Hermann J 1999 *J. Appl. Phys.* **86** 6096
[6] Amoruso S 1999 *Appl. Phys.* A **69** 323
[7] Wood R F, Leboeuf J N, Geohegan D B, Puretzky A A and Chen K R 1998 *Phys. Rev.* B **58** 1533
[8] Lu Y F, Hong M H and Low T S 1999 *J. Appl. Phys.* **85** 2899
[9] Park S M, Chae H, Wee S and Lee I 1998 *J. Chem. Phys.* **109** 928
[10] Harilal S S, Issac R C, Bindhu C V, Nampoori V P N and Vallabhan C P G 1997 *J. Phys. D: Appl. Phys.* **30** 1703
[11] Harilal S S, Bindhu C V, Nampoori V P N and Vallabhan C P G 1998 *Appl. Phys. Lett.* **72** 167
[12] Kennedy E T *et al* 1994 *Opt. Eng.* **33** 3984
[13] Harilal S S, Issac R C, Bindhu C V, Nampoori V P N and Vallabhan C P G 1997 *J. Appl. Phys.* **81** 3637
[14] Harilal S S, Bindhu C V, Issac R C, Nampoori V P N and Vallabhan C P G 1997 *J. Appl. Phys.* **82** 2140
[15] Liu H C, Mao X L, Yoo J H and Russo R E 1999 *Spectrochim. Acta* B **54** 1607
[16] Andreic Z, Aschke L and Kunze H-J 1998 *J. Phys. D: Appl. Phys* **31** 1487
[17] Issac R C, Harilal S S, Bindhu C V, Nampoori V P N and Vallabhan C P G 1997 *Spectrochim. Acta* B **52** 1791
[18] Mayo R M, Newman J W, Sharma A, Yamagata Y and Narayan J 1999 *J. Appl. Phys.* **86** 2865
[19] Nagata Y, Midorikawa K, Kubodera S, Obara M, Tashiro H and Toyoda K 1993 *Phys. Rev. Lett.* **71** 3774
[20] Ditmire T *et al* 1995 *Phys. Rev.* A **51** R4337
[21] Chaker M, Lafontaine B, Cote C Y, Kieffer J C, Pepin H, Talon M H, Enright G D and Villeneuve D M 1992 *J. Vac. Sci. Technol.* B **10** 3239
[22] Irons F E and Peacock N J 1973 *J. Phys. E: Sci. Instrum.* **6** 857
[23] Doehring T, Stiehler J, Boweing N and Heinzmann U 1994 *J. Phys. B: At. Mol. Opt. Phys.* **27** L663
[24] Iglesias E J and Griem H R 1988 *Phys. Rev.* A **38** 308
[25] Sailaja S, Arora V, Kumbhare S R, Naik P A, Gupta P D, Fedin D A, Rupasov A A and Shikanov A S 1998 *Meas. Sci. Technol.* **9** 1462
[26] Sailaja S, Arora V, Kumbhare S R, Naik P A and Gupta P D 1998 *Opt. Laser Technol.* **30** 407
[27] Boland B C, Irons F E and Mcwhirter R W P 1968 *J. Phys. B: At. Mol. Phys.* **1** 1180
[28] Irons F E, Mcwhirter R W P and Peacock N J 1972 *J. Phys. B: At. Mol. Phys.* **5** 1975
[29] Miyazaki K and Takada H 1995 *Phys. Rev.* A **52** 3007
[30] Atwee T, Aschke L and Kunze H J 2000 *J. Phys. D: Appl. Phys.* **33** 2263
[31] Kelly R and Dreyfus R W 1988 *Nucl. Instrum. Methods* B **32** 341
[32] Singh R K and Narayan J 1990 *Phys. Rev.* B **41** 8843
[33] Singh R K, Holland O W and Narayan J 1990 *J. Appl. Phys.* **68** 233
[34] Angleraud B, Aubreton J and Catherinot A 1999 *Eur. Phys. J.* AP **5** 303
[35] Nishikawa T, Nakano H, Uesugi N, Nakao M and Masuda H 1999 *Appl. Phys. Lett.* **75** 4079
[36] http://physics.nist.gov/PhysRefData/contents.html
[37] http://cfa-www.harvard.edu/amdata/ampdata/kelly/kelly.html
[38] Griem H R 1964 *Plasma Spectroscopy* (New York: McGraw-Hill)
[39] Harilal S S, Bindhu C V, Nampoori V P N and Vallabhan C P G 1998 *Appl. Phys.* B **66** 633
[40] Gamaly E G, Rode A V and Luther-Davies B 1999 *Appl. Phys.* A **69** S121
[41] Gamaly E G 1994 *Laser Part. Beams* **12** 185
[42] Kruer W L 1988 *The Physics of Laser Plasma Interactions* (New York: Addison-Wesley)
[43] Hora H 1991 *Plasmas at High Temperature and Density* (Heidelberg: Springer-Verlag)
[44] Tuebner U, Bergmann J, van Wonterghem B and Schäfer F P 1993 *Phys. Rev. Lett.* **70** 794
[45] Borghesi M, Mackinnon A J, Gaillard R, Willi O and Riley D 1999 *Phys. Rev.* E **60** 7374
[46] Zel'dovitch Y B and Raizer Y P 1966 *Physics of Shock Waves and High Temperature Hydrodynamic Phenomena* (New York: Academic)
[47] Amoruso S, Armenante M, Berardi V, Bruzzese R and Spinelli N 1997 *Appl. Phys.* A **65** 265